ACS APPLIED MATERIALS & INTERFACES

Research Article

www.acsami.org

Low-Temperature Preparation of Ag-Doped ZnO Nanowire Arrays, DFT Study, and Application to Light-Emitting Diode

Thierry Pauporté,*[,†] Oleg Lupan,[†,‡] Jie Zhang,[†] Tugba Tugsuz,[†] Ilaria Ciofini,[†] Frédéric Labat,[†] and Bruno Viana[†]

[†]Institut de Recherche de Chimie–Paris, CNRS–Chimie ParisTech–PSL, UMR8247, 11 rue Pierre et Marie Curie, 75005 Paris, France

[‡]Department of Microelectronics and Biomedical Engineering, Technical University of Moldova, 168 Stefan cel Mare Boulevard, Chisinau MD-2004, Republic of Moldova

Supporting Information

ABSTRACT: Doping ZnO nanowires (NWs) by group IB elements is an important challenge for integrating nanostructures into functional devices with better and tuned performances. The growth of Ag-doped ZnO NWs by electrodeposition at 90 °C using a chloride bath and molecular oxygen precursor is reported. Ag acts as an electrocatalyst for the deposition and influences the nucleation and growth of the structures. The silver atomic concentration in the wires is controlled by the additive concentration in the deposition bath and a content up to 3.7 atomic % is reported. XRD analysis shows that the integration of silver enlarges the lattice parameters of ZnO. The optical measurements also show that the direct optical bandgap of ZnO is reduced by silver doping. The bandgap shift and lattice expansion are explained by first principle calculations using the density functional theory (DFT) on the silver impurity integration as an interstitial (Ag_i) and as a substitute of zinc atom (Ag_{Zn}) in the crystal lattice. They notably indicate that Ag_{Zn} doping forms an impurity band because of Ag 4d and O 2p orbital interactions, shifting the Fermi level toward the valence band. At least, Ag-doped ZnO vertically aligned nanowire arrays have been epitaxially grown on GaN(001) substrate. The heterostructure has been inserted in a light emitting device. UV-blue light emission has been achieved with a low emission threshold of 5 V and a tunable red-shifted emission spectrum related to the bandgap reduction induced by silver doping of the ZnO emitter material.

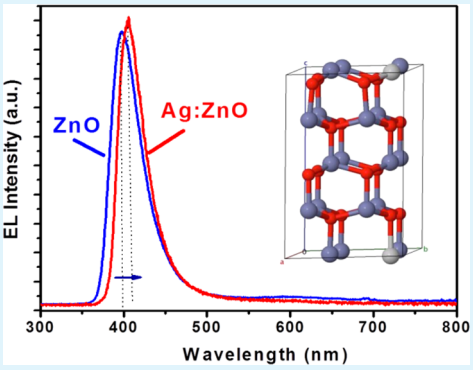

KEYWORDS: *ZnO, electrodeposition, light-emitting diode, Ag-doping, DFT modeling, UV–blue emission*

1. INTRODUCTION

Zinc oxide is a key material for advanced applications in the fields of nano- and microtechnologies.[1−4] This oxide is characterized by a wide direct bandgap of 3.37 eV at room temperature and a strong exciton binding energy of 60 meV.[1−4] It can be grown with various tunable nano/microstructures such as nanowires (NWs) and nanorods (NRs)[1,5,6] and can be doped by various elements.[7−12] A broad spectrum of tunable properties have been reported by doping ZnO at various levels.[7−24] They include high transparency, conductivity ranging from the metallic to the insulating ones, piezoelectricity,[2] selective sensitivity,[7] photocatalytic properties,[8] ferromagnetic properties,[9,10] and important magneto-optic effects.[11,12]

ZnO NW and NR array layers have attracted a tremendous attention due to various interesting properties related to their low-dimensionality, optical, and confinement effects and large surface to volume ratio.[1,5,6,25] They can be grown by various techniques using the vapor or the liquid phase.[1] Among the latter, many reports have focused on the sol–gel method, the hydrothermal growth, the chemical bath deposition and the electrodeposition. ZnO structures of high structural and optical quality have been prepared by electrochemical deposition at rather low temperatures.[1,2] Moreover, the heteroepitaxial growth has been successfully demonstrated on various conducting single crystals and the preparation of electrodeposited ZnO emitters for near-UV light emitting diodes (LED) application has been published by our group.[26,27] Moreover, we have shown that transition metal-doping of ZnO permits the adjustment of the light emission spectrum of the device.[28−31] Both red-shifted[28,29] and blue-shifted[31] LED emissions by electrochemical doping have been obtained depending on the cation additive dissolved in the electrodeposition bath.

Doping ZnO by the group-IB elements is of special interest since theoretical studies have shown that the defect formation energies of substitutional group-IB elements (Cu, Ag and Au) are low.[32−34] This is especially the case when Ag substitutes Zn

Received: February 15, 2015
Accepted: May 20, 2015
Published: May 20, 2015

DOI: 10.1021/acsami.5b01496
ACS Appl. Mater. Interfaces 2015, 7, 11871−11880

atoms in the lattice to give Ag_{Zn} which is stable compared to Ag-doping in an interstitial site (Ag_i). The calculated Ag_{Zn} transition energy is located only 0.4 eV above the ZnO valence band maximum (VBM) and could act, theoretically, as an efficient acceptor for p-type doping.[32] Moreover, the high ionization energy of the group-IB elements may also be used for bandgap engineering. The low formation energy of substitutional group-IB element indicates that high concentration of defect can be integrated in ZnO. A defect band can form inside the ZnO bandgap, leading to its narrowing.[32] The large p−d coupling between the oxygen p state and the Ag d state suggests that the effective mass of the defect band will be small and improve the transport properties.[32] The preparations of Ag-doped ZnO layers, nanostructured or not, by various deposition techniques using the vapor phase such as pulsed laser deposition,[17] magnetron sputtering,[18−20] e-beam evaporation,[22] metal−organic chemical vapor deposition,[21] or solutions[23,24] have been reported in the literature. On the other hand, the electrochemical deposition of Ag-doped ZnO nanostructures has been very poorly explored[14−16] with the notable exception of the work by Cui and co-workers who have shown that the electrochemical preparation of p-type ZnO:Ag structures is possible by using very accurate deposition conditions and a nitrate precursor.[14,15]

In our previous papers, copper, a group-IB element of small size, has been successfully incorporated in the crystal lattice of ZnO NWs and NRs by the electrochemical growth technique using $CuCl_2$ additives in the electrodeposition bath.[27,28] Copper cation was incorporated in the ZnO lattice at an atomic concentration higher than the initial one in the solution. We also showed that doping gave rise to a bandgap reduction. The p-type doping was not observed likely because of the native donor defect compensation.

In the present work, the effect of silver additive on the electrochemical growth of ZnO-NWs in a chloride bath has been thoroughly investigated. Ag-doped ZnO NW arrays have been produced and the obtained material has been extensively characterized. A ZnO bandgap reduction is observed. The experimental data have been explained in the light of the theoretical investigation of the system using DFT computational calculations. The electrodeposited ZnO:Ag NWs have been also successfully grown on p-GaN crystals and a LED structure has been prepared. The n-ZnO:Ag NWs/p-GaN epitaxial heterojunction under forward bias polarization was characterized by an electroluminescence peak centered in the near UV−blue spectral region and red-shifted compared to the structures prepared with pure ZnO NW emitters.

2. EXPERIMENTAL SECTION

2.1. ZnO Layer Preparation. The deposition was performed at 90 °C in a classical three-electrode electrochemical cell using a solution containing 0.2 mM $ZnCl_2$, 0.1 M KCl as supporting electrolyte, and continuous bubbling of oxygen in a bath solution.[35,36] Different concentrations of $AgNO_3$ (99.9%, Alfa Aesar) have been utilized, namely 0.5, 1, and 2 μM. Glass sheet substrates coated with polycrystalline F-doped SnO_2 (FTO) and having a resistance of 10 Ω/□ were used as a working electrode (WE). Before the deposition, they were ultrasonicated sequentially in acetone, then in ethanol for 6 min each. After a rinsing step under an abundant deionized (DI) water (18.2 MΩ cm) flow, they were ultrasonicated in HNO_3 (45%) for 2 min, then in DI water for 5 min and finally dried under an air flux.

The electrodeposition was carried out at constant applied potential using an Autolab PGSTAT30 potentiostat/galvanostat monitored by the GPES AutoLab software. The reference was a Saturated Calomel Electrode (SCE). Upon deposition, the substrate was rotated at a constant speed of ω = 300 rotations/min (rpm). After deposition, the layers were abundantly rinsed with DI water and dried in air. The deposited layers were finally annealed in air at 250 °C for 12 h.

The epitaxial ZnO NWs were grown on p-type Mg-doped GaN(001) layers supported on sapphire (TDI, Inc. corporation) according to the procedure described elsewhere.[26] The deposition time was 3600 s. The heterojunction was annealed 12 h at 250 °C before to be included in the LED device as described in our previous works.[26−30]

2.2. ZnO Layer Characterizations. The sample morphological properties were studied with an Ultra 55 Zeiss FEG scanning electron microscope (SEM) at an acceleration voltage of 10 kV. Quantitative elemental analyses (EDX) were realized with a Bruker Li-drift silicon detector. The XRD patterns were determined by a Phillips X'pert high-resolution X-ray diffractometer operated at 40 kV and 45 mA using the CuKα radiation with λ = 1.54060 Å and a rotating sample holder. The optical characterization of pure ZnO and ZnO:Ag nanowire arrays was performed in the wavelength range from 300 to 800 nm using a Varian Cary 5000 spectrophotometer equipped with an integrating sphere. The reference was a FTO coated glass sheet cleaned exactly with the same procedure as the samples. The photoluminescence (PL) and electroluminescence (EL) spectra were measured as described elsewhere.[28]

2.3. DFT Modeling. The Ag-doping of wurtzite ZnO was theoretically characterized by periodic calculations carried out at the DFT level using the CRYSTAL09 code,[37] which computes the electronic structure of systems within Hartree−Fock (HF), DFT, and hybrid HF/DFT approximations using Gaussian-type orbitals as basis set, thus allowing to efficiently use hybrid functionals for band structure calculations. The PBE0 functional,[38] mixing 25% of HF exchange in a PBE scheme, has been used throughout.

Silver doping was investigated both by Zn-substitution and Ag-insertion. For the substitution calculations, three different Ag doping amounts were considered: 0.78, 1.85, and 6.25 at %, by substituting one Zn site in neutral (4 × 4 × 4), (3 × 3 × 3), and (2 × 2 × 2) supercells, respectively. Because the Zn-substituted supercells are neutral, they contain an odd number of electrons, so that an open-shell formalism has been considered for all substitution calculations. On the other hand, insertion of closed shell Ag^+ has only been investigated for the 1.85 at % case, and a closed-shell formalism has been taken into account. For the sake of clarity, in the following, the compact notations Ag_{Zn} and Ag_i will be used to define Zn substitution and Ag insertion, respectively.

All ZnO:Ag calculations were performed with 6 k points in the irreducible part of the Brillouin zones (IBZ) of the above-mentioned supercells, whereas reference calculations were also performed on pure ZnO with 28 k points in the IBZ. All structures were fully relaxed (lattice parameters and atomic positions) using default convergence criteria.[37] A pruned (75,974) integration grid was used in all DFT calculations.

The following basis sets were used: oxygen atoms were described with a Durand and Barthelat large core pseudopotential, the $2s^22p^4$ electrons being explicitly taken into account with a (4s4p) → [2s2p] contraction scheme; a Hay and Wadt large core pseudopotential combined to a (3s3p5d) → [3s3p2d] contraction scheme for the $3d^{10}4s^2$ electrons were considered for zinc atoms. On the other hand, an all-electron basis set was used for Ag with the following contraction scheme: (27s18p11d)→ [6s5p3d]. This level of theory has already proven to provide reliable geometrical and electronic properties of ZnO-based systems.[39]

3. RESULTS AND DISCUSSION

3.1. Electrochemical Study of the Deposition. Figure 1a, b shows the current curves recorded upon the first and second cyclic voltammetry (CV) scans, respectively, measured at the FTO substrate electrode rotated at 300 rpm. The bath was composed of zinc chloride at 0.2 mM, a supporting electrolyte (KCl) at 0.1 M and O_2 at saturation. O_2 gas was

DOI: 10.1021/acsami.5b01496
ACS Appl. Mater. Interfaces 2015, 7, 11871−11880

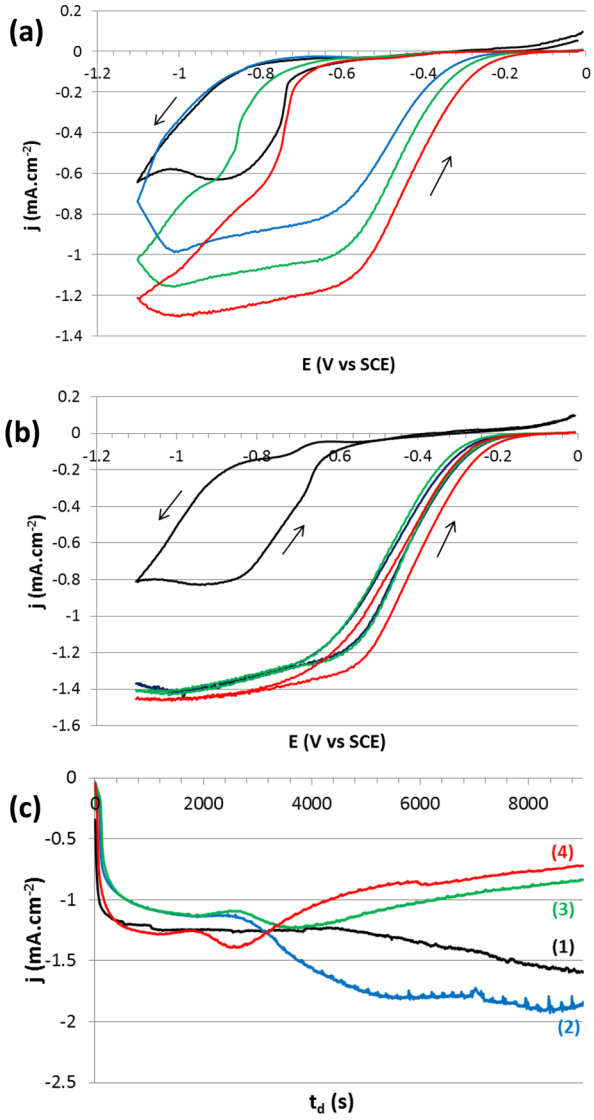

Figure 1. (a) First and (b) second voltammetry cycles recorded on the FTO substrate in the ZnO electrodeposition solutions with various $AgNO_3$ concentrations: (black) 0 μM, (blue) 0.5 μM, (green) 1 μM, and (red) 2 μM. Scan rate 10 mV s^{-1}, T = 90 °C. (c) Growth curves at constant applied potential. T = 90 °C.((1, black) 0 μM $AgNO_3$, −1.0 V vs SCE; ((2, blue) 0.5 μM $AgNO_3$, −0.70 V vs SCE; ((3, green) 1 μM $AgNO_3$, −0.57 V vs SCE; and ((4, red) 2 μM $AgNO_3$, −0.57 V vs SCE.

Table 1. Initial Cation Concentration, [Ag(I)]/[Zn(II)] Ratio Present in the Electrolyte and Final Atomic Ag-Content in the ZnO:Ag Nanowires Measured by EDX in Layers Deposited for 9000 s

Initial [$AgNO_3$] in the aqueous electrolyte (μM)	[Ag(I)]/[Zn(II)] ratio in the starting aqueous electrolyte (%)	E_{appl} (V) vs SCE	Atomic Ag content determined by EDX (%)[a]
0	0.0	−1.0	0.0
0.5	0.25	−0.70	0.9
1	0.5	−0.57	1.8
2	1	−0.57	3.7

[a]Defined as the [Ag]/ [Ag+Zn] ratio.

continuously bubbled upon the current measurement and the bath temperature was maintained at 90 °C. Without silver ions,

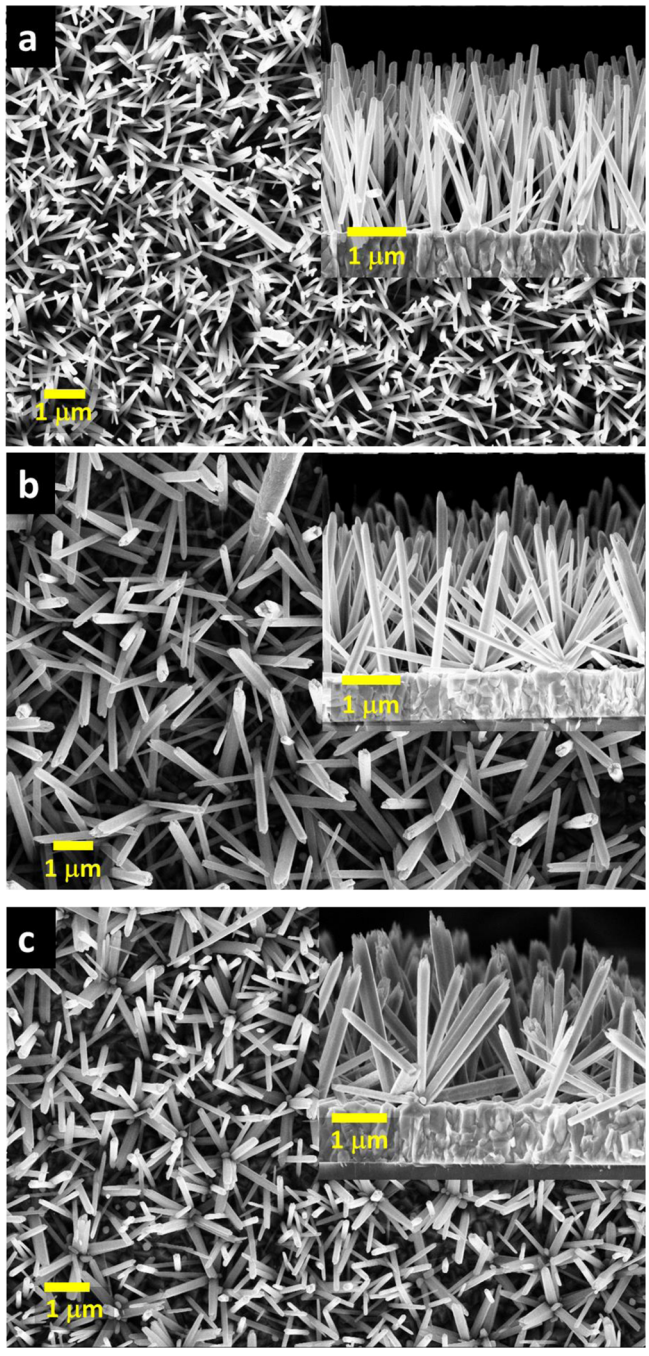

Figure 2. SEM images of (a) pure ZnO NWs and Ag-doped ZnO NWs grown with (b) 1 μM $AgNO_3$ and (c) 2 μM $AgNO_3$. The insets show the cross-sectional views of the wire arrays.

a cathodic wave appeared at −0.8 V which increased upon the negative-going scan. After the potential scan reversion, a higher current was measured which rapidly decreased above −0.85 V. Adding $AgNO_3$ in the solution had a dramatic effect on the measured current, even if the concentrations used in the present work were very low. We also observed a substantial increase in the cathodic current with the concentration of silver ion present in the bath. Ag acts as an electrocatalyst for the electrochemical reaction and then for the deposition of the layer. The CV curves were different for the second scan presented in Figure 1b. If a higher current was recorded for pure ZnO, a large curve hysteresis was still present. The CV in

DOI: 10.1021/acsami.5b01496
ACS Appl. Mater. Interfaces 2015, 7, 11871−11880

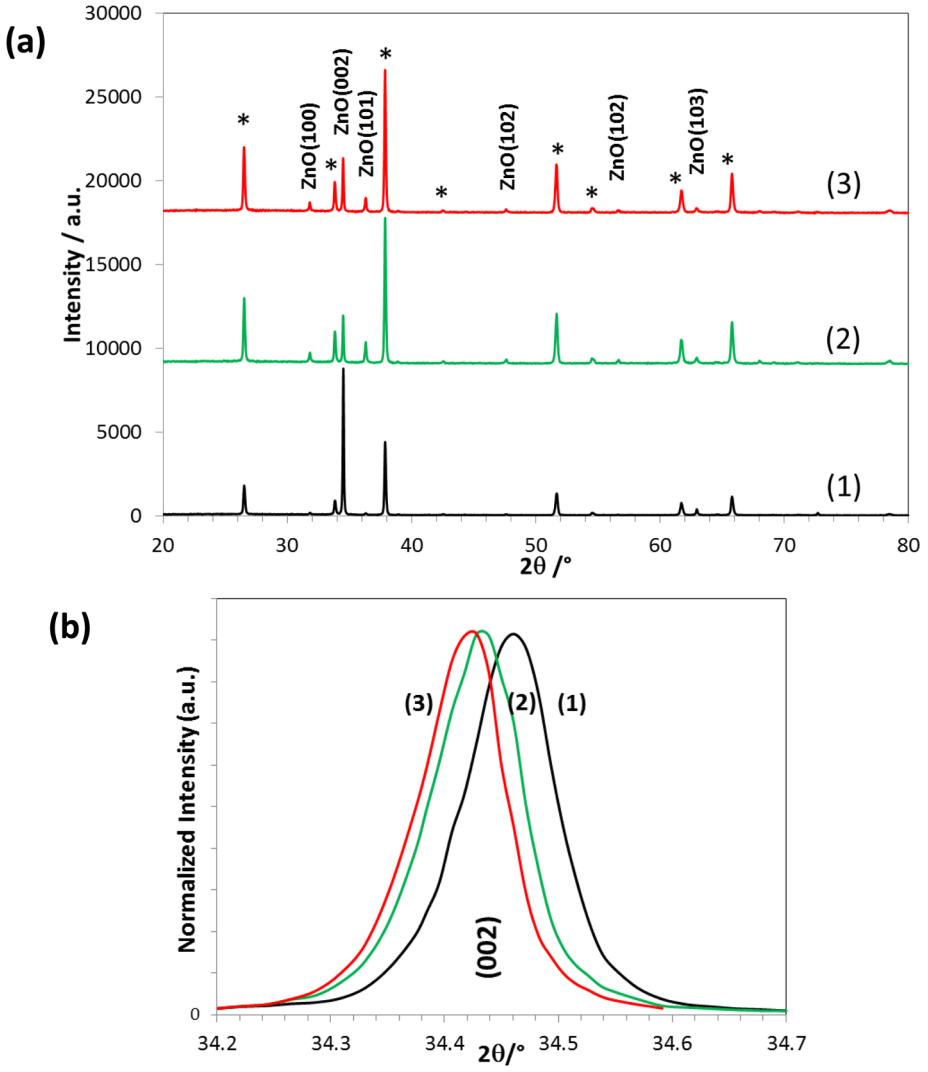

Figure 3. (a) XRD patterns of the ZnO nanowire arrays doped with Ag (*: reflection peaks of FTO substrate). (b) Zoom view of the (002) peaks from XRD pattern of pure ZnO nanowire arrays and ZnO doped with Ag. (1) 0 μM, (2) 1 μM, and (3) 2 μM $AgNO_3$.

Table 2. Effect of $AgNO_3$ Concentration on the Lattice and FWHM XRD Parameters Obtained for the ZnO(100) and ZnO(002) Diffraction Peaks

initial [$AgNO_3$] in the aqueous electrolyte (μM)	(h k l) planes	2θ (deg)	[fwhm] (deg)	c- and a-parameters (nm)
0	(100)	31.81	0.149	0.52009
	(002)	34.46	0.0967	0.32456
1	(100)	31.80	0.151	0.52053
	(002)	34.43	0.0958	0.32466
2	(100)	31.80	0.175	0.52068
	(002)	34.42	0.0908	0.32466

the presence of silver reaches a plateau at j_{max} ~1.4 mA cm^{-2}. Its value did not depend on the concentration of silver in the bath and the plateau extended over 0.5 V. The observed cathodic current waves are due to the electrochemical reduction of molecular oxygen: $O_2 + 2H_2O + 4e^- \rightarrow 4OH^-$. The reaction generates hydroxide ions at the electrode surface and ZnO is precipitated due to the pH increase.[40] The large hysteresis in Figure 1a shows that ZnO is more electroactive for that reaction compared to the bare FTO substrate. During the second scan, more ZnO is present at the electrode surface and

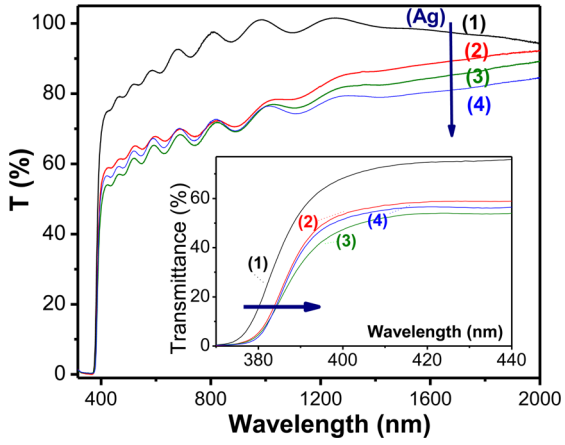

Figure 4. Optical total transmission curves and (inset) zoom-view of the band-edge. ZnO NWs electrodeposition with four different concentrations of $AgNO_3$ in the bath: curve 1, pure ZnO NWs; 2, ZnO:Ag (0.5 μM); 3, ZnO:Ag (1 μM); and 4, ZnO:Ag (2 μM).

then more current is generated. In the presence of silver, the codeposition of silver also occurs. Because of the low concentration of this additive, this element is incorporated in

DOI: 10.1021/acsami.5b01496
ACS Appl. Mater. Interfaces 2015, 7, 11871−11880

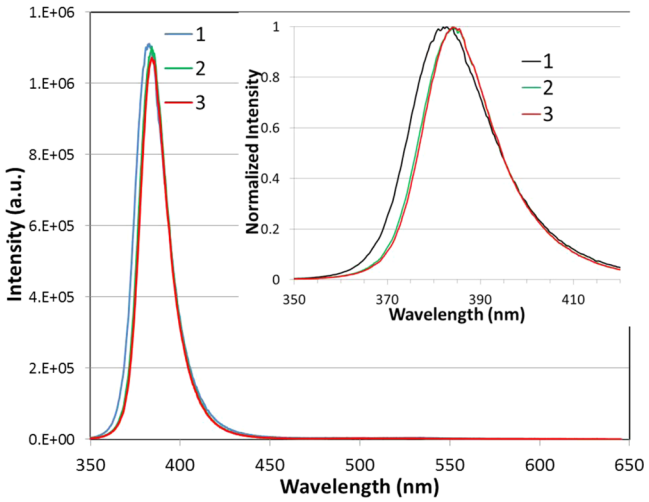

Figure 5. Room-temperature photoluminescence spectra of ZnO and ZnO:Ag Nanowires. (1) 0 μM $AgNO_3$, (2) 1 μM $AgNO_3$, and (3) 2 μM $AgNO_3$. Excitation wavelength of 266 nm.

Table 3. Computed Effects of Silver Doping on the Wurtzite Lattice Parameters (*a*, *b*, *c*, α (angle between the *b* and *c* axis), β (angle between the *a* and *c* axis), and γ (angle between the *a* and *b* axis)) and Zinc/Silver to Oxygen Distances; Electronic Gaps of the Systems Computed for α and β Spins, Respectively (E_{gap}^{α}, E_{gap}^{β})

	pure ZnO	Ag_{Zn}			Ag_i
at % Ag	0.00	0.78	1.85	6.25	1.85
a (Å)	3.331	3.336	3.343	3.343	3.496
b (Å)]	3.331	3.336	3.343	3.398	3.497
c (Å)	5.178	5.176	5.169	5.177	5.737
α (deg)	90.00	90.00	90.00	90.00	90.00
β (deg)	90.00	90.00	90.00	89.66	90.00
γ (deg)	120.00	120.00	120.00	120.55	120.01
$Zn/Ag-O_1$ (Å)	2.005	2.221	2.212	2.256	2.441
$Zn/Ag-O_2$ (Å)	2.005	2.221	2.212	2.125	2.507
$Zn/Ag-O_3$ (Å)	2.005	2.221	2.212	2.125	2.586
$Zn/Ag-O_4$ (Å)	2.005	2.169	2.167	2.271	2.507
E_{gap}^{α} (eV)	3.93	3.74	3.60	3.72	3.20
E_{gap}^{β} (eV)	3.93	1.93	1.79	0.24	3.20

the ZnO lattice and surface. During the first scan, the measured current is higher compared to the pure ZnO bath because the silver atoms on the deposit surface catalyze the molecular oxygen electroreduction reaction. For the second scan, the plateau and the low curve hysteresis in the presence of silver is due to a limitation of the deposition reaction by the diffusion of molecular oxygen.

On the basis of these curves, we have prepared layers at constant applied voltage. The applied potential was adjusted for each investigated $AgNO_3$ concentration in order to take into account the variable electroactivity of the deposited structure and is disclosed in Table 1. The current transient curves are shown in Figure 1c. Without silver or at low silver ion concentration, the current increases first before to reach a plateau. After more than 2200 s of deposition, a slow increase is observed that is likely due to the wire growth and then to the increase in the electrode surface area. However, in the case of higher concentrations of silver ions, the current had the tendency to decrease after several thousands of seconds of deposition time.

3.2. Morphological and Structural Properties. Representative SEM images of layers prepared at various silver ion concentrations and deposited for 9000s are presented in Figure 2. In the absence of silver ion additive, they are made of arrayed self-standing thin ZnO NWs which are well vertically oriented and directly grown on the FTO substrate (Figure 2a). They have a typical diameter of 100−120 nm and a length of 2.8−3.1 μm. Their length increased with the deposition time. Changes in the deposit characteristics were observed in the presence of silver in the electrolyte. The nucleation was more difficult in this case since arrays of wires grown from the same point are observed forming flower-like structures (Figure 2b, c).[1] A consequence is the presence of inclined long wires and a less texturation of the deposits. Only wires are observed without the presence of a secondary structure. With increasing silver ion concentration, the density of flowers increased as well as the number of wires grown from the same initial nucleus. Because silver acts as an electrocatalyst, increasing $AgNO_3$ favors the hydroxide ion generation at the beginning of the growth and consequently the supersaturation is promoted. This enhances the nucleation and the density of wires. Chemical analyses by X-ray energy-dispersive spectroscopy (EDX) have been conducted in order to estimate the atomic Ag content of the layers grown at various silver nitrate concentrations. The results of EDX analysis are reported in Table 1. A continuous increase is found with the additive concentration and a concentration of about 3.7% is measured in wires grown in the presence of 2 μM $AgNO_3$. We can note that the silver/zinc atomic ratio is significantly higher in the deposited material compared to in the initial deposition medium (Table 1).

The XRD patterns of the layers are presented in Figure 3. They are indexed by the wurtzite hexagonal phase of ZnO for the layers prepared in the presence or not of silver. The reflections due to the FTO substrate are also observed marked with an asterisk (*) in Figure 3a. The patterns show the overexpression of the (002) plane. This is especially the case for the pure ZnO layers which is composed of well-vertically oriented NWs (Figure 2a). There was no evidence of crystallized silver-based impurity phase at these Ag doping concentrations. A zoom view of the (002) reflection peak shows a shift toward a lower angle with the silver bath content (Figure 3b). The lattice parameters have been determined and are gathered in Table 2. A lattice expansion is observed with the presence of silver, especially in the c-direction (Table 2 and Figure S1 of the Supporting Information. Many other studies in the literature have described the expansion of the ZnO lattice due to the integration of silver dopant.[20,23,41−43] It is assigned to the radius of Ag^+ (126 pm) or Ag^{2+}(97 pm) which is much larger than that of Zn^{2+} (74 nm).[44] The substitution of zinc by silver will then result in a lattice expansion. The increase is mainly observed between 0 μM and 1 μM. The integration of silver then looks more difficult for the highest concentrations investigated.

3.3. Optical Properties. Figure 4 shows the UV−visible transmission spectra of the ZnO layers for different atomic % of Ag. They are characterized by an absorption edge in the near-UV. The pure ZnO sample is highly transparent with a transmittance maximum close to 100% in the near-IR region. In the presence of Ag, the transparency decreases. Increasing the dopant content reduces the transparency in the infrared region. The zoom of the band-edge (Figure 4 inset) shows a shift

DOI: 10.1021/acsami.5b01496
ACS Appl. Mater. Interfaces 2015, 7, 11871−11880

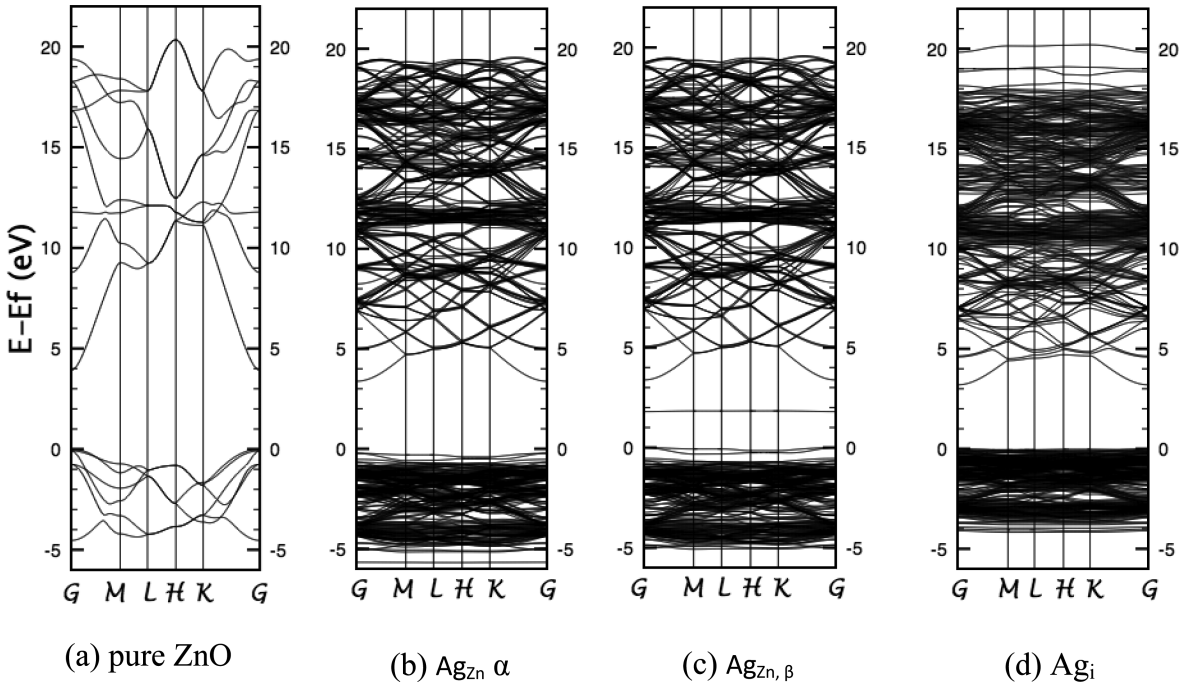

Figure 6. Computed band structures for (a) pure ZnO, (b) α and (c) β spins of the Ag_{Zn} system at 1.85 at %, and (d) Ag_i at 1.85 at %.

toward longer wavelengths from 384 to 388 nm and then a slight optical bandgap reduction in agreement with other investigations on Ag-doped layers prepared by other deposition techniques.[19] In their study, Jeong et al.[44] observed a gradual shift of the optical gap as a function of Ag content. The bandgap narrowed down with increasing Ag content and the reason was the substitution of zinc by silver.[44] In our experiment, this shift is less marked, but our observation is in agreement with previous work.[44]

The photoluminescence (PL) spectra have been measured at room temperature and are presented in Figure 5. The wires are characterized by a strong near-band edge emission in the near-UV−violet wavelength region. It is remarkable that no visible emission due to bulk and surface defects is observed either for the pure ZnO or Ag-doped ZnO nanowires. The NWs are of very high structural quality even if the deposition temperature is only 90 °C. The excitonic PL emission is slightly shifted toward a longer wavelength by several nm with the doping with silver and the PL emission is about the same with 1 μM and 2 μM $AgNO_3$ additive concentrations. The intensity of the near-UV emission is similar with and without Ag doping in NWs. In the presence of Ag the fwhm of this emission is reduced. The room temperature PL characteristics of the samples show the excellent structural quality of the material electrodeposited in the presence of $AgNO_3$ in the electrochemical bath. For both transmittance and PL spectra, the shift effect is the more pronounced for the lowest concentrations investigated. It suggests that the integration of silver atoms in the lattice at high concentration is rather difficult by the technique.

3.4. Theoretical Study. According to the experimental data discussed above, it is clear that the doping of ZnO with Ag affects both the host lattice geometry and electronic structure. To support and get insights on this experimental evidence, hybrid DFT calculations have been performed on: (i) pure ZnO; (ii) ZnO:Ag, both considering Zn_{Ag} at three different doping amounts (0.78, 1.85, and 6.25 at %) and Ag_i, only at the 1.85 at % amount. Results are gathered in Table 3, and the unit cells of all systems are represented in Figure S2 in the Supporting Information.

From a geometrical point of view, it is clear that insertion of Ag in the wurtzite lattice has a stronger effect than substitution of one Zn for one Ag. This can be evidenced from the stronger increases of the lattice parameters when going from the pure ZnO system to the Ag_i one than to the Ag_{Zn} ones, the largest effect being computed on c (+10.8%). Similar conclusions, already drawn in previous theoretical works,[15,45] are qualitatively in line with the experimental data presented in this work (see Table 2). This is also confirmed by the four metal/oxygen distances reported in Table 3, which are significantly larger in the insertion case than in the substitution cases, regardless of the doping level considered. As already mentioned in the Section 3.2, this can be directly ascribed to the larger radius of Ag when compared to Zn. In addition, the regular tetrahedron found around Zn in pure ZnO is distorted upon Ag doping. For instance, when considering substitution with the two lowest doping amounts, three long and one short Ag−O distances are obtained, outlining the distortion due to a Jahn−Teller effect.

The presence of Ag in the host's lattice strongly affects the computed band gaps. When Ag is inserted, the band gap is reduced from 3.93 to 3.20 eV, the doped system remaining a large band gap semiconductor. On the other hand, when substitution is considered, significant differences are obtained for α and β electrons. Indeed, while the α band gap decreases only slightly from the pure ZnO value (from 3.93 eV to a minimum of 3.60 eV), the β band gap is much more affected, with computed values decreasing with the increase of the doping amount, reaching 0.24 eV when a 6.25 at % amount is considered. These findings can be further explained by the combined analysis of spin density plots, band structures and density of states. In particular, the analysis of the valence band edge (VBE) and conduction band edge (CBE) composition allows getting some insights on the rise of a p-type ZnO material upon doping. Because for the Ag_{Zn} case, spin density

DOI: 10.1021/acsami.5b01496
ACS Appl. Mater. Interfaces 2015, 7, 11871−11880

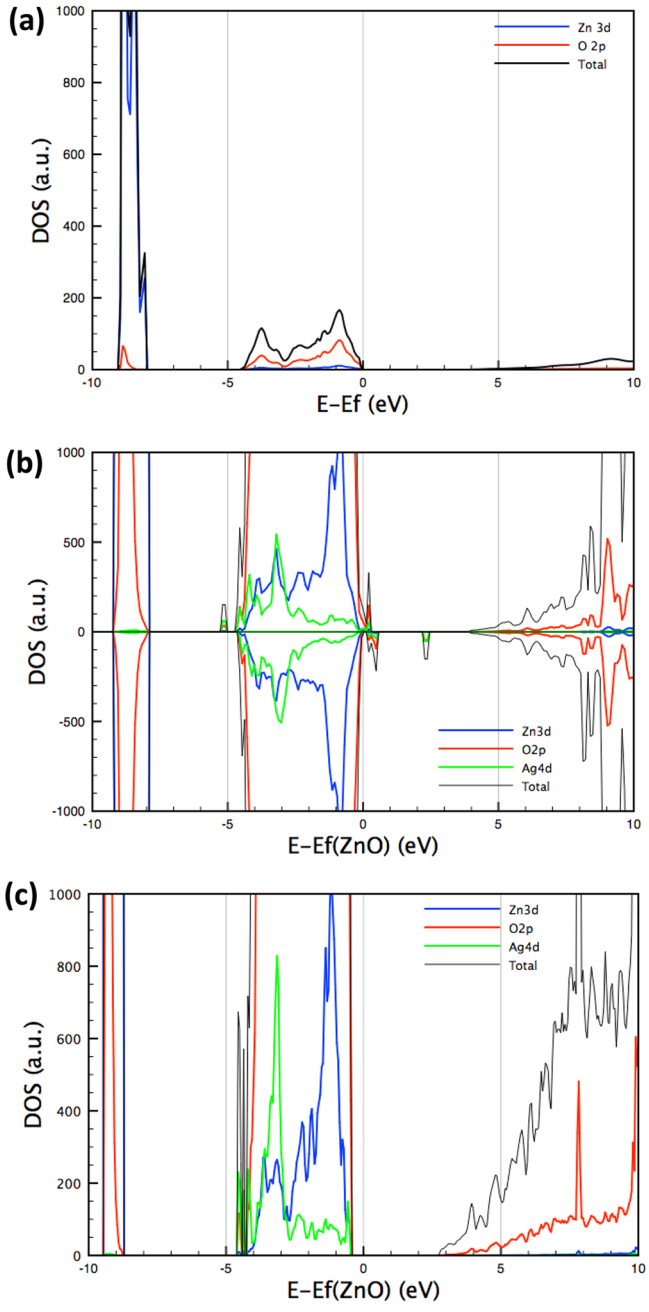

Figure 7. Computed total and orbital-projected density of states for (a) pure ZnO, (b) Ag_{Zn}, 1.85 at%. The upper and lower panels correspond to α and β spins, respectively, and (c) Ag_i systems at 1.85 at %. The Fermi level of the pure ZnO system is set at 0 eV.

localization, band structures, and density of states are qualitatively similar for all doping amounts considered, in the following, we discuss only data obtained at the 1.85 at % doping amount.

The spin density plotted in Figure S3 (Supporting Information) in the Ag_{Zn} case reveals that the α contribution is mainly localized on the Ag atom, with small contributions on neighboring O atoms, consistent with a formal Ag^{2+} cation (d^9), for which three long and one short Ag−O distances are obtained because of a Jahn−Teller effect (see Table 3). As expected, this confirms the modification of the ZnO electronic structure upon Ag doping, where electronic states deriving from Ag should be found at the VBE. From the computed band

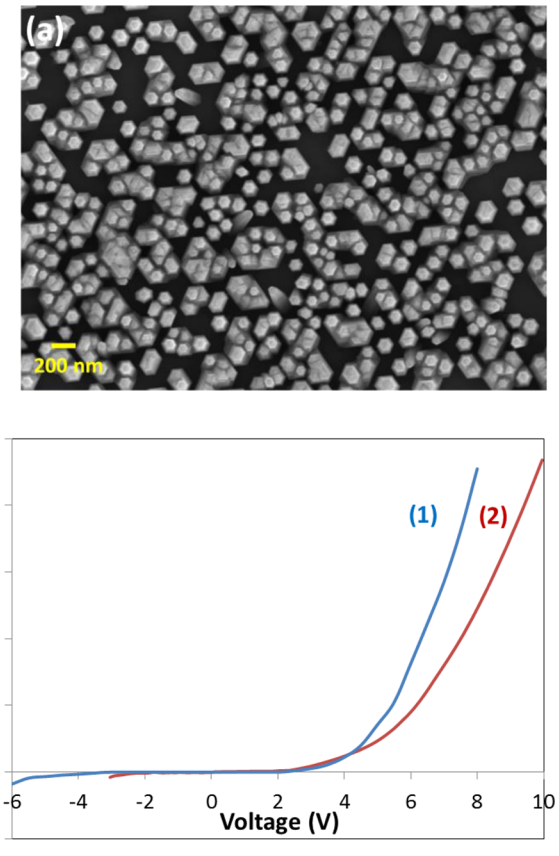

Figure 8. (a) FE-SEM top view of electrodeposited ZnO:Ag (1 μM) on p-GaN(001). (b) Current−voltage curves of heterojunction LED prepared with (1) 0 μM and (2) 1 μM $AgNO_3$.

structures reported in Figure 6, it can be evidenced that the band gap remains direct at Γ in all cases considered. Moreover, in the Ag_{Zn} case, it is clear that the band gap reduction is related to the introduction of energy levels in the ZnO band gap (Figure 7b). Comparison of the total and orbital-projected density of states (DOS) of pure ZnO and Ag_{Zn} of Figure 7 indeed reveals that, upon Ag doping, the Zn_{3d}/O_{2p} hybridization found at the VBE for pure ZnO is replaced by Ag_{4d}/O_{2p} hybridization both for α and β spins, whereas the CBE for the β spins is now due to the introduction of a new level in the ZnO band gap, mainly derived from Ag_{4d} levels. This is qualitatively in line with previous theoretical works (see refs 15 and 45 for instance). In the case of interstitial doping (Ag_i), on the other hand, no shallow levels deriving from the dopant are obtained in the ZnO band gap, only a significant contribution of Ag_{4d} being observed at the top of the valence band. Hence the qualitative picture that we get from these calculations is that p-type ZnO is formed when Ag substitutes for one Zn, with a shallow level found in the ZnO band gap, only 0.24 eV above the VBE when a 6.25 at % doping amount is considered. This should then theoretically allow better transport properties of Ag-doped ZnO when compared to pure ZnO. When Ag is inserted, however, no shallow state is found above the VBE, and thus no p-type ZnO is obtained.

3.5. Application to LED Structures. The deposition of Ag-doped ZnO has been performed in a bath containing 1 μM of $AgNO_3$, using a p-type Mg-doped GaN(001) layer supported on sapphire. For this experiment we shifted the deposition applied potential to a more negative value of −1.2 V/SCE. The current density was about the same as on FTO, namely

DOI: 10.1021/acsami.5b01496
ACS Appl. Mater. Interfaces 2015, 7, 11871−11880

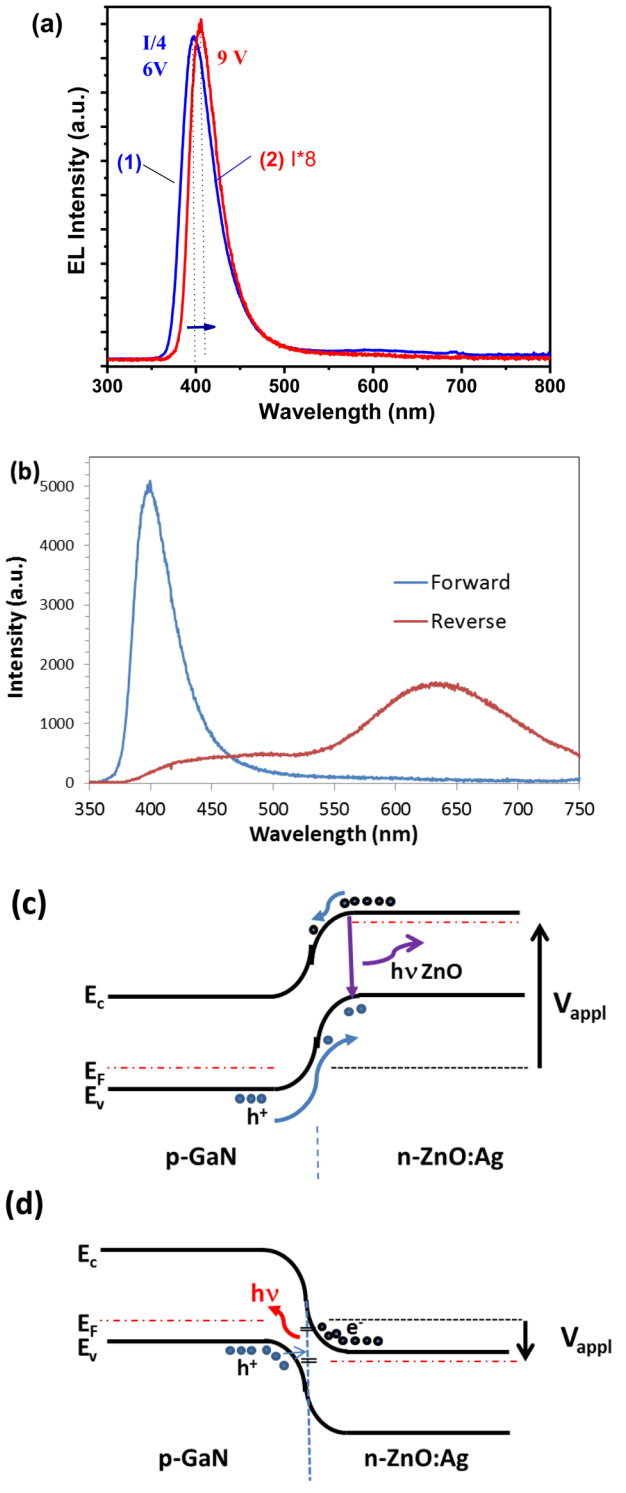

Figure 9. (a) Room-temperature electroluminescence (EL) spectra of pure ZnO NWs/p-GaN (curve 1) and Ag-doped ZnO NWs/p-GaN (curve 2) (1 μM $AgNO_3$ in the bath) under forward bias. (b) Comparison of the EL spectra of ZnO:Ag (1 μM)/p-GaN measured under forward and reverse bias (same 0.9 mA current). (c) Energy band diagram of light emission under forward applied bias. (d) Energy band diagram of light emission under reverse applied bias.

measured at −1.2:−1.3 mA cm^{-2} and constant throughout the deposition process. The deposition time was 1 h. A top SEM view of the layer in Figure 8a shows hexagonal nanorods grown on the smooth single-crystalline p-GaN surface. As described in previous works,[26,46] the fact that the hexagonal facets have the same orientation for all the crystallites is the signature that ZnO is grown epitaxially on the *c*-plane of GaN with the same in-plane orientation.[26,46] The heterostructure has been used to prepare a LED as described elsewhere.[26,27] The *I*−*V* curves are presented in Figure 8b. They show a rectifying behavior and a lower current was measured for the Ag-doped ZnO based LED. The LED structure was forward biased at room temperature and it was observed a slightly larger emission turn-on voltage (>5 V) of the LED structure based on Ag-doped ZnO compared to with pure ZnO-NWs/GaN (4.4 V).[26] The threshold remained very low and demonstrated the high quality of the interfaces in the ZnO:Ag NW-based LED. Our results confirm the ability of electrochemical growth techniques to give high quality ZnO NWs and good interfaces on *p*-GaN. Above 8 V, the violet-blue emission could be observed with the naked eye. The emission spectra for both the pure and Ag-doped ZnO based devices under a forward bias voltage of 6 and 9 V, respectively, are compared in Figure 9a. The emission was red-shifted in the presence of silver. Indeed, a shift of the emission peak from 397 nm up to 406 nm was observed. The shift suggests that the emission due to the band-to-band recombination of holes and electrons occurs in ZnO and that the wavelength is significantly lengthened for the Ag-doped ZnO due to a reduced bandgap. In Figure 9a, no visible emission in the green-red region was measured either for pure or Ag-doped emitters, showing the high structural quality of the heterostructure. We can note that very recently Echresh et al. have published ZnO:Ag/p-GaN LEDs prepared by chemical deposition.[47] In their case, the emission threshold voltage was clearly higher and both a UV-blue and a visible emission centered at 660 nm were reported due to the presence of defects in the deposited Ag-doped ZnO material.

Our results show a wavelength emission shift by about 0.17 eV for ZnO:Ag between the peak observed experimentally in the EL of the diodes (Figure 9a) and in the PL spectra (Figure 5). This is classically observed for ZnO/GaN LED and in our previous work,[26,27] a similar shift was found between PL and EL (~0.12 eV) measured from pure ZnO/*p*-GaN structure in exactly the same experimental conditions. PL is measured from the top part of the ZnO nanowires and is determined by the energetic structure of the NW material. On the other hand, EL emission is generated by carrier recombination at the near-interface between the two semiconductors and is influenced by the energy properties of the ZnO/GaN heterojunction, notably by the energy offset between the conduction and the valence bands of ZnO and GaN (Figure 9c). We can also mention that because of the current flow in the device, the temperature of the emitting material may vary between the two experiments.

In Figure 9b, the EL emission is compared under the forward and the reverse bias measured for the same flowing current. The emission spectra are completely different. Under forward applied bias, the emission is characterized by a single UV-blue peak. The emission wavelength is sensitive to the ZnO doping so it suggests that the band-to-band recombinations occur in ZnO near the interface according to the mechanism presented in Figure 9c. Under reverse bias, the main emission peak is centered in the red region at 633 nm. The most probable mechanim for that emission is shown in Figure 9d. The junction is in an accumulation regime which favors the radiative recombinations through defects present near the interface.[48] The rectifying behavior observed for the heterostructure suggests that the deposited ZnO:Ag structures have a n-type

DOI: 10.1021/acsami.5b01496
ACS Appl. Mater. Interfaces 2015, 7, 11871−11880

conductivity and that p-type conducting ZnO by Ag-doping was not achieved in our case. It is assigned to native donor defect compensation. We have confirmed this observation by preparing electrodeposited ZnO:Ag NW arrays on n-type GaN single crystal substrates. After integration of these layers in a LED structure, no UV-blue EL emission peak could be detected.

4. CONCLUSIONS

We have reported the growth of Ag-doped ZnO NW by electrodeposition at 90 °C using a chloride bath and molecular oxygen precursor. Ag acts as an electrocatalyst for the cathodic deposition. SEM studies reveal the presence of long NW without the presence of a visible secondary phase and a less texturation of the deposits. According to SEM images, with increasing silver ion concentration, the density of wires increases as well as the number of NW grown from the same initial nucleus. A zoom view of the (002) XRD reflection peak shows a shift toward a lower angle with the silver bath content. The lattice parameters have been determined and a lattice expansion is found with the presence of silver, especially in the *c*-direction. UV−visible transmission spectra of the ZnO layers with increasing atomic % of Ag in NWs show that the transparency decreases in the infrared region. The excitonic PL emission demonstrates a slight shift toward longer wavelengths from 384 to 388 nm and the transmittance curves show a slight optical bandgap reduction. First principle calculations using the density functional theory (DFT) have been performed to understand the effect of Ag doping on the structural, electronic, and optical properties of ZnO. According to DFT theoretical calculations a better transport property of Ag-doped ZnO, when compared to pure ZnO, is expected. When Ag is substituted to Zn, the qualitative picture from calculations predicts that p-type ZnO is formed, with a shallow acceptor state found in the ZnO band gap, only 0.24 eV above the VBE. The bandgap reduction is also predicted as well as a lattice expansion, in good agreement with the experimental results. Heterostructures have been used to prepare a LED. The *I*−*V* curves showed a rectifying behavior and a lower current was measured for the Ag-doped ZnO/GaN-based devices. The LED structure forward biased presented a relatively low emission threshold turn-on voltage at ∼5 V and above 8 V, the violet-blue emission could be observed with the naked eye. The EL emission was red-shifted in the presence of silver dopant in ZnO NW. p-type ZnO was not observed experimentally due to native donor defect compensation. Our results present a first step forward toward practical applications of Ag-doped ZnO NW-based devices for light emission application.

■ ASSOCIATED CONTENT

Supporting Information

Variation in the ZnO lattice parameters with the $AgNO_3$ concentration; fully relaxed unit cells of the substituted systems and computed spin density of the Ag_{Zn} system. The Supporting Information is available free of charge on the ACS Publications website at DOI: 10.1021/acsami.5b01496.

■ AUTHOR INFORMATION

Corresponding Author

*E-mail: thierry.pauporte@chimie-paristech.fr.

Notes

The authors declare no competing financial interest.

■ ACKNOWLEDGMENTS

This work was partly supported by the STCU through Grant 5989.

■ REFERENCES

(1) Pauporté, T. Preparation of ZnO Nanorods and Nanowires by Wet Chemistry. In *Wide Band Gap Semiconductor Nanowires for Optical Devices: The Particular Case of GaN and ZnO*; Feuillet, G., Consonni, V., Eds.; Wiley-ISTE: Arlington, VA, 2014; pp 325−378.
(2) Ozgur, U.; Alivov, Y. I.; Liu, C.; Teke, A.; Reshchikov, M. A.; Dogan, S.; Avrutin, V.; Cho, S. J.; Morkoc, H. A. Comprehensive Review of ZnO Materials and Devices. *J. Appl. Phys.* **2005**, *98*, 041301.
(3) Janotti, A.; Van de Walle, C. G. Fundamentals of Zinc Oxide as a Semiconductor. *Rep. Prog. Phys.* **2009**, *72*, 126501.
(4) Gudiksen, M. S.; Lauhon, L. J.; Wang, J.; Smith, D. C.; Lieber, C. M. Growth of Nanowire Superlattice Structures for Nanoscale Photonics and Electronics. *Nature* **2002**, *415*, 617.
(5) Guérin, V. M.; Pauporté, T. From Nanowires to Hierarchical Structures of Template-Free Electrodeposited ZnO for Efficient Dye-Sensitized Solar Cells. *Energy Environ. Sci.* **2011**, *4*, 2971−2979.
(6) Hosni, H.; Kusumawati, Y.; Farhat, S.; Jouini, N.; Pauporté, T. Effects of Oxide Nanoparticle Size and Shape on Electronic Structure, Charge Transport and Recombination in Dye-Sensitized Solar Cell Photoelectrodes. *J. Phys. Chem. C* **2014**, *118*, 16791−16798.
(7) Lupan, O.; Chow, L.; Pauporté, T.; Ono, L. K.; Roldan Cuenya, B.; Chai, G. Highly Sensititive and Selective Hydrogen Single Nanowire Sensor Operating at Room Temperature. *Sens. Actuators, B* **2012**, *173*, 772−780.
(8) Wang, W.; Xin, J. H.; Yang; Yang; Liu, H.; Xu, L.; Hu, J. The Characteristics and Photocatalytic activities of Silver Doped ZnO Nanocrystallites. *Appl. Surf. Sci.* **2004**, *227*, 312−317.
(9) Liu, C.; Yun, F.; Morkoc, H. Ferromagnetism of ZnO and GaN: A Review. *J. Mater. Sci.: Mater. Electron.* **2005**, *16*, 555−597.
(10) Macdonald, A. H.; Schiffer, P.; Samarth, N. Ferromagnetic Semiconductors: Moving Beyond (Ga, Mn)As. *Nat. Mater.* **2005**, *4*, 195−202.
(11) Lambrecht, W. R. L.; Rodina, A. V.; Limpijumnong, S.; Segall, B.; Meyer, B. K. Valence-Band Ordering and Magneto-Optic Exciton Fine Structure in ZnO. *Phys. Rev. B* **2002**, *65*, 075207.
(12) Behan, A. J.; Neal, J. R.; Ibrahim, R. M.; Mokhtari, A.; Ziese, M.; Blythe, H. J.; Fox, A. M.; Gehring, G. A. Magneto-Optical and Transport Studies of ZnO-Based Dilute Magnetic Semiconductors. *J. Magn. Magn. Mater.* **2007**, *310*, 2158−2160.
(13) Reynolds, J. G.; Reynolds, C. L. Progress in ZnO Acceptor Doping: What Is the Best Strategy? *Adv. Condens. Matter Phys.* **2014**, 457058.
(14) Thomas, M. A.; Cui, J. B. Electrochemical Route to p-Type Doping of ZnO Nanowires. *J. Phys. Chem. Lett.* **2010**, *1*, 1090−1094.
(15) Thomas, M. A.; Sun, W. W.; Cui, J. B. Mechanism of Ag Doping in ZnO Nanowires by Electrodeposition: Experimental and Theoretical Insights. *J. Phys. Chem. C* **2012**, *116*, 6383−6391.
(16) Fu, M.; Li, S. L.; Yao, J.; Wu, H. P.; He, D. W.; Wang, Y. S. Preparation and Characterization of Electrodeposited Ag-Doped ZnO Inverse Opals with a Smooth Surface. *J. Porous Mater.* **2013**, *20*, 1485−1489.
(17) Kang, H. S.; Ahn, B. D.; Kim, J. H.; Kim, G. H.; Lim, S. H.; Chang, H. W.; Lee, S. Y. Structural, Electrical and Optical Properties of p-type ZnO thin Films with Ag dopant. *Appl. Phys. Lett.* **2006**, *88*, 202108.
(18) Chen, Y.; Xu, X. L.; Zhang, G. H.; Xue, H.; Ma, S. Y. A Comparative Study of the Microstructures and Optical Properties of Cu- and Ag-doped ZnO Thin Films. *Physica B* **2009**, *404*, 3645−3649.
(19) Sahu, D. R. Studies of the Properties of Sputter Deposited Ag-doped ZnO Films. *Microelectron. J.* **2007**, *38*, 1252−1256.
(20) Duan, L.; Lin, B.; Zhang, W.; Zhong, S.; Fu, Z. Enhancement of Ultraviolet Emission from ZnO Films by Ag-Doping. *Appl. Phys. Lett.* **2006**, *88*, 232110.

DOI: 10.1021/acsami.5b01496
ACS Appl. Mater. Interfaces 2015, 7, 11871−11880

(21) Khomchenko, V. S.; Kryshtab, T. G.; Savin, A. K.; Zavyalova, L. V.; Roshchina, N. N.; Rodionov, V. E.; Lytvyn, O. S.; Kushnirenko; Khachatryan, V. B.; Andraca-Adame, J. A. Fabrication and Properties of ZnO:Cu and ZnO:Ag Thin Films. *Superlattices Microstruct.* **2007**, *42*, 94−98.
(22) Kim, I. S.; Jeong, E. K.; Kim, D. Y.; Kumar, M.; Choi, S. Y. Investigation of p-Type Behavior in Ag-doped ZnO Thin Films by E-beam Evaporation. *Appl. Surf. Sci.* **2009**, *255*, 4011−4014.
(23) Lupan, O.; Chow, L.; Ono, L. K.; Roldan Cuenya, B.; Chai, G.; Khallaf, H.; Park, S.; Schulte, A. Synthesis and Characterization of Ag- and Sb-Doped ZnO Nanorods by a Facile Hydrothermal Route. *J. Phys. Chem. C* **2010**, *114*, 12401−12408.
(24) Duan, L.; Zhang, W. X.; Yu, X. C.; Wang, P.; Jiang, Z. Q.; Luan, L. J.; Chen, Y. N.; Li, D. L. Stable p-type ZnO Films Dual-Doped with Silver and Nitrogen. *Solid State Commun.* **2013**, *157*, 45−48.
(25) Hsu, C. L.; Chang, S. J. Doped ZnO 1D Nanostructures: Synthesis, Properties, and Photodetector Application. *Small* **2014**, *10*, 4562−4585.
(26) Lupan, O.; Pauporté, T.; Viana, B.; Tiginyanu, I. M.; Ursaki, V. V.; Cortès, R. Epitaxial Electrodeposition of ZnO Nanowire Arrays on p-GaN for Efficient UV-Light Emitting Diode Fabrication. *ACS Appl. Mater. Interfaces* **2010**, *2*, 2083−2090.
(27) Lupan, O.; Pauporté, T.; Viana, B. Low-voltage UV-Electroluminescence from ZnO-Nanowire Array/ p-GaN Light Emitting Diodes. *Adv. Mater.* **2010**, *22*, 3298−3302.
(28) Lupan, O.; Pauporté, T.; Le Bahers, T.; Viana, B.; Ciofini, I. Wavelength Emission Tuning of ZnO Nanowires-based Light Emitting Diodes by Cu-doping: Experimental and Computational Insights. *Adv. Funct. Mater.* **2011**, *21*, 3564−3572.
(29) Lupan, O.; Pauporté, T.; Viana, B.; Aschehoug, P. Electrodeposition of Cu-Doped ZnO Nanowire Arrays and Heterojunction Formation with p-GaN for Color Tunable Light Emitting Diode Applications. *Electrochim. Acta* **2011**, *56*, 10543−10549.
(30) Lupan, O.; Pauporté, T.; Le Bahers, T.; Ciofini, I.; Viana, B. High Aspect Ratio Ternary $Zn_{1-x}Cd_xO$ Nanowires by Electrodeposition for Light Emitting Diode Application. *J. Phys. Chem. C* **2011**, *115*, 14548−14558.
(31) Lupan, O.; Viana, B.; Pauporté, T.; Dhaouadi, M.; Pellé, F.; Devis, L.; Gacoin, T. Controlled Mixed Violet/blue-Red Electroluminescence from Eu:NanoPhosphors/ZnO-nanowires/p-GaN Light Emitting Diodes Light Emitting Diodes. *J. Phys. Chem. C* **2013**, *117*, 26768−26775.
(32) Yan, Y.; Al-Jassim, M. M.; Wei, S. H. Doping of ZnO by Group-IB Elements. *Appl. Phys. Lett.* **2006**, *89*, 181912.
(33) Li, Y.; Zhao, X.; Fan, W. Structural, Electronic and Optical Properties of Ag-Doped ZnO Nanowires: First Principles Study. *J. Phys. Chem. C* **2011**, *115*, 3552−3557.
(34) Chai, G.; Lin, C.; Wang, J.; Zhang, M.; Wei, J.; Cheng, W. Density Functional Theory Simulations of Structures and Properties for Ag-Doped ZnO Nanotubes. *J. Phys. Chem. C* **2011**, *115*, 2907−2913.
(35) Elbelghiti, H.; Pauporté, T.; Lincot, D. Mechanistic Study of ZnO Nanorod Array Electrodeposition. *Phys. Status Solidi A* **2008**, *205*, 2360−2364.
(36) Pauporté, T.; Bataille, G.; Joulaud, L.; Vermersch, F. J. Well-Aligned ZnO Nanowire Arrays Prepared by Seed Layer-Free Electrodeposition and their Cassie-Wenzel Transition after Hydrophobization. *J. Phys. Chem. C* **2010**, *114*, 194−202.
(37) Saunders, V. R.; Dovesi, R.; Roetti, C.; Orlando, R.; Zicovich-Wilson,C. M.; Harrison, N. M.; Doll, K.; Civalleri, B.; Bush, I.; D'Arco, P.; Llunell, M. *Crystal 09 User's Manual*; Universita di Torino: Torino, Italy, 2009.
(38) Adamo, C.; Barone, V. Toward Reliable Density Functional Methods Without Adjustable Parameters: The PBE0 Model. *J. Chem. Phys.* **1999**, *110*, 6158.
(39) Labat, F.; Ciofini, I.; Adamo, C. Modeling ZnO Phases Using a Periodic Approach: From Bulk to Surface and Beyond. *J. Chem. Phys.* **2009**, *131*, 044708.
(40) Goux, A.; Pauporté, T.; Lincot, D. Oxygen Reduction on Zinc Oxide Electrodes in KCl Aqueous Solution at 70°C. *Electrochim. Acta* **2006**, *51*, 3168−3172.
(41) Deng, R.; Zou, Y. M.; Tang, H. G. Correlation Between Electrical, Optical Properties and Ag^{2+} Centers of ZnO:Ag Thin Films. *Physica B* **2008**, *403*, 2004−2007.
(42) Duan, L.; Gao, W.; Chen, R. Q.; Fu, Z. X. Influence of Post-Annealing Conditions on Properties of ZnO:Ag Films. *Solid State Commun.* **2008**, *145*, 449−481.
(43) Deng, R.; Yao, B.; Li, Y. F.; Yang, T.; Li, B. H.; Zhang, Z. Z.; Shan, C. X.; Zhang, J. Y.; Shen, D. Z. Influence of Oxygen/Argon Ratio on Structural, Electrical and Optical Properties of Ag-doped ZnO Thin Films. *J. Cryst. Growth* **2010**, *312*, 1813−1816.
(44) Jeong, S. H.; Park, B. N.; Lee, S. B.; Boo, J. H. Structural and Optical Properties of Silver-Doped Zinc Oxide Sputtered Films. *Surf. Coat. Technol.* **2005**, *193*, 340−344.
(45) Zhang, X. D.; Guo, M. L.; Shen, Y. Y.; Liu, C. L.; Xue, Y. H.; Zhu, F.; Zhang, L. H. Electronic Structure and Optical Transition in Heavy Metal Doped ZnO by First-Principle Calculations. *Comput. Mater. Sci.* **2012**, *54*, 75−80.
(46) Pauporté, T.; Lincot, D. Heteroepitaxial Electrodeposition of Zinc Oxide on Gallium Nitride. *Appl. Phys. Lett.* **1999**, *75*, 3817−3820.
(47) Echresh, A.; Chey, C. O.; Shoushtari, M. Z.; Nur, O.; Willander, M. Tuning the Emission of ZnO Nanorods Based Light Emitting Diodes Using Ag Doping. *J. Appl. Phys.* **2014**, *116*, 193104.
(48) Lupan, O.; Pauporté, T.; Viana, B. Low-Temperature Growth of ZnO Nanowire Arrays on p-Silicon (111) for Visible-Light-Emitting Diode Fabrication. *J. Phys. Chem. C* **2010**, *114*, 14781−14785.

DOI: 10.1021/acsami.5b01496
ACS Appl. Mater. Interfaces 2015, 7, 11871−11880